

## TERAHERTZ GRID FREQUENCY DOUBLERS

Jung-Chih Chiao<sup>1</sup>, Andrea Markelz<sup>2</sup>, Yongjun Li<sup>3</sup>, Jonathan Hacker<sup>4</sup>,  
Thomas Crowe<sup>3</sup>, James Allen<sup>2</sup>, and David Rutledge<sup>1</sup>

<sup>1</sup>Department of Electrical Engineering, California Institute of Technology, Pasadena, CA 91125

<sup>2</sup>Department of Physics, University of California at Santa Barbara, Santa Barbara, CA 93106

<sup>3</sup>Department of Electrical Engineering, University of Virginia, Charlottesville, VA 22903

<sup>4</sup>Bellcore Communications Research, Red Bank, NJ 07701

**Abstract** – A terahertz quasi-optical grid frequency doubler has been developed. This frequency doubler is a planar bow-tie grid structure periodically loaded with planar Schottky diodes. This is the first experimental result with quasi-optical grid frequency multipliers in the terahertz frequency range. A peak output power of  $330 \mu\text{W}$  was measured at 1 THz for  $2.42 \mu\text{s}$  500-GHz input pulses with a peak power of 3.3 W.

### INTRODUCTION

The demand for solid-state local oscillators in the THz frequency range has been steadily increasing for applications in radio astronomy and remote sensing of the atmosphere [1,2]. The interest for THz applications has fostered a strong need for submillimeter-wave receivers, mixers and sources, especially tunable high-power sources used as the local oscillators for heterodyne submillimeter-wave receivers. For example, the local-oscillator output-power requirement at 1 THz for NASA's SMMM (Submillimeter Moderate Mission) is at least  $50 \mu\text{W}$  [3]. Traditional high-power sources in the THz region such as gas lasers and vacuum-tube oscillators are not suitable for this purpose due to their large size, high-voltage supplies, short lifetime

and small tuning ranges. However, frequency multipliers and upconverters like Schottky diode multipliers can be used to generate the required terahertz frequencies from lower-frequency solid-state tunable signal sources such as Gunn-diode oscillators.

### APPROACH

Current diode multipliers have mostly been single-diode structures typically consisting of a Schottky varactor diode placed in a waveguide with a whisker contact. Rydberg, Lyons and Lidholm have demonstrated a Schottky varactor diode frequency tripler with a measured output power more than  $120 \mu\text{W}$  at 803 GHz [4]. Erickson and Tuovinen presented a waveguide tripler with an output power of  $110 \mu\text{W}$  at 800 GHz [5]. Zimmermann, Rose and Crowe have demonstrated an output power of  $60 \mu\text{W}$  at 1 THz by using a cascade of two whisker contacted Schottky varactor frequency triplers [6]. One approach to overcome the low power of solid-state devices in the submillimeter-wave band is to combine a large number of devices together [7,8]. A grid of planar diodes quasi-optically coupled in free space does not require the construction of single-mode waveguides and can potentially overcome the power limits of conventional single-diode multipliers [9]. Using this approach, H.-X. Liu has demonstrated a frequency

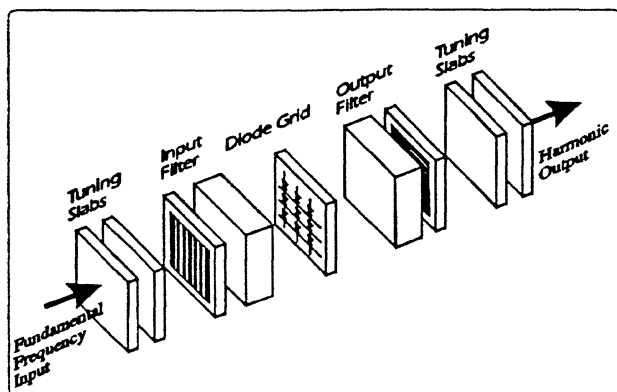


Fig. 1. The grid-multiplier concept [8]. The fundamental wave enters on the left as a beam, passes through a filter, and is incident on the diode grid. The grid acts as a nonlinear surface and produces a beam at the harmonic frequencies, which passes through filters on the right.

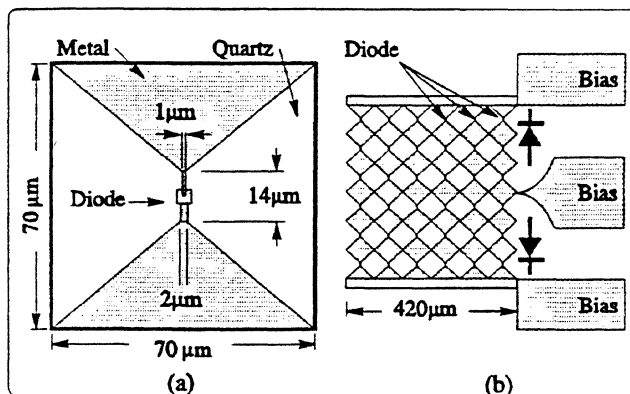


Fig. 2. The grid frequency doubler. (a): the unit cell, (b): the entire  $6 \times 6$  array. The diode symbols indicate the polarity. Three diodes are in series from the top or bottom bias line to the center bias line. The bow-ties in two adjacent columns are not connected except the ones in the center row for biasing.

tripler consisting of 3,100 Schottky-quantum-barrier varactor diodes to produce 5 W pulsed output power at 99 GHz [10].

The multiplier concept is shown in Fig. 1. The input beam at the fundamental frequency enters from the left. The first element is a pair of dielectric tuning slabs that act to transform the impedance of the input wave to one appropriate for the multiplier grid. Typically inductive reactance is needed to cancel capacitance of the diodes in the grid. In addition, the free-space wave impedance,  $377 \Omega$ , is inconveniently high and needs to be reduced. Next the beam passes through a low-pass filter that passes the fundamental frequency, but reflects harmonics. Then the beam hits the grid. The grid acts as a nonlinear surface which results from the nonlinearity of I-V or C-V characteristics of diodes and generates harmonics. This harmonic beam radiates both forward and backward, but the

backward beam reflects off the low-pass filter. The forward beam passes through the high-pass filter, and then through another pair of tuning slabs. One important feature is that the tuning slabs are outside the filters, so that the input and output can be tuned independently. The entire structure is quite compact, only a few wavelengths thick. The design is also suitable for cascading, so that even higher harmonics could be produced. The multiplication process preserves the beam shape. Therefore, a focused beam could be used so that different sizes of multiplier grids could be cascaded.

In this paper, the tuning slabs were not used for experimental simplicity.

### PLANAR SCHOTTKY DIODE GRID

These grid multipliers were fabricated by monolithic technology on a  $30\text{-}\mu\text{m}$  thick fused-quartz substrate at the University of Virginia [11]. Figure 2(a) shows the bow-tie-shaped metal pattern used for the unit cell. The Schottky diode junction is located at the center of the unit cell. The size of a unit cell is  $70\text{ }\mu\text{m} \times 70\text{ }\mu\text{m}$ . Figure 2(b) shows the entire  $6 \times 6$  array. The active area is  $420\text{ }\mu\text{m} \times 420\text{ }\mu\text{m}$ . Three diodes are in series from the top or bottom bias line to the center bias line. The adjacent bow-ties are not connected except the center row. The diodes in the top and bottom halves of the grid have opposite polarity. This is because the grid was originally designed as a sideband generator[7]. When the grid is used as a frequency multiplier, the polarity change causes an undesired null in the middle of the beam.

Figure 3(a) shows an SEM picture of the planar Schottky diode located between the metal fingers of the bow-tie structure. Figure 3(b) and 3(c) show the top view and the cross section of the planar Schottky diode. The anode has a diameter of  $0.5\text{ }\mu\text{m}$ . The n-GaAs layer has a thickness of  $0.1\text{ }\mu\text{m}$  and a doping concentration of  $4 \times 10^{17}\text{ cm}^{-3}$ .

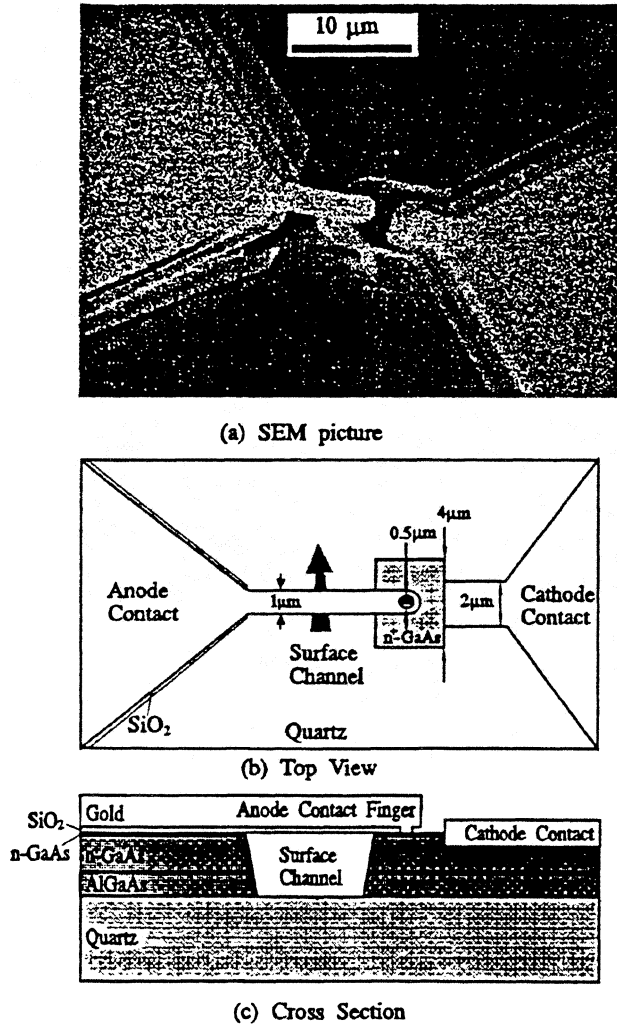


Fig. 3. (a) The SEM picture, (b) the top view and dimensions, and (c) the cross section of the Schottky diode.

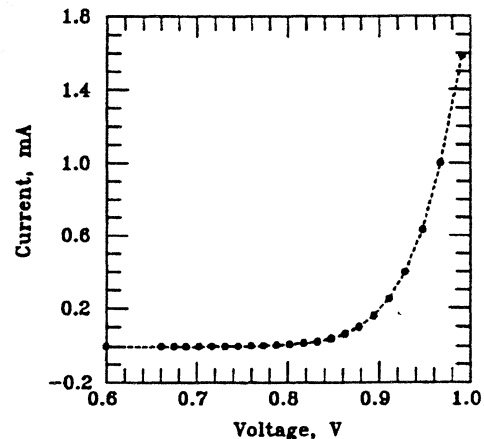


Fig. 4. Typical measured DC I-V curve.

The  $n^+$ -GaAs layer has a thickness of  $3\ \mu\text{m}$  and a doping concentration of  $5 \times 10^{18}\text{cm}^{-3}$ . The AlGaAs layer has a thickness of  $1.5\ \mu\text{m}$ . A surface channel was etched away underneath the anode contact finger to reduce the shunt capacitance. The diodes have a measured DC series resistance of  $14\ \Omega$  and an estimated junction capacitance of  $0.6\ \text{fF}$  at zero bias. Figure 4 shows a typical I-V curve measured on one of the diodes.

## MEASUREMENT ARRANGEMENT

The measurements use the free-electron laser (FEL) as the input source in the Quantum Institute at the University of California, Santa Barbara. The free-electron laser generates kilowatts of polarized radiation tunable from 120 GHz to 4.8 THz [12]. The pulse width is  $2.42\ \mu\text{s}$  with a period of 1.3 s. The measurement setup is shown in Fig. 5. All the optical components were aligned using a He-Ne laser. Half of the input power at the fundamental frequency in the incident beam was split off into a reference detector. We used a pyroelectric detector as the reference detector. The radiation from the FEL was then focused by a parabolic mirror with an f-number of 1.6 and a focal length of 15 cm. We varied the input power by inserting plexiglass attenuators in front of the beam splitter.

The harmonic radiation from the grid was collimated by an f/1 parabolic mirror with a focal length of 11 cm. A metallic-mesh Fabry-Perot interferometer in the collimated beam was used to measure the frequency content. The diameter of the interferometer is 15 cm so that it covers the

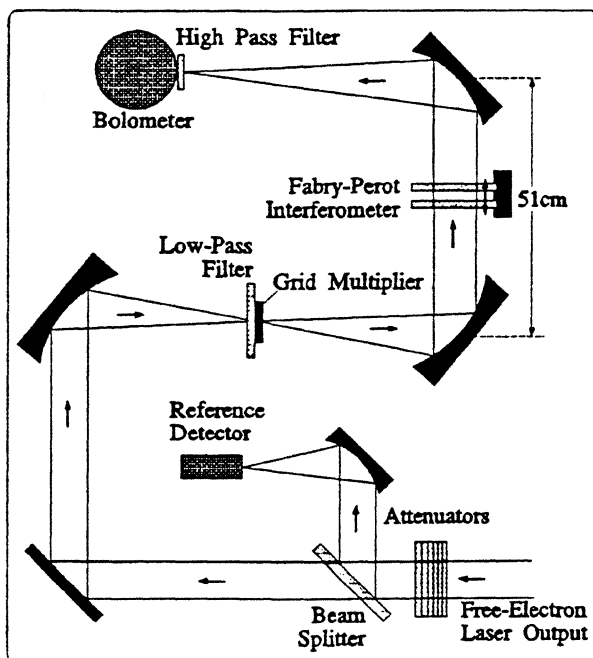


Fig. 5. Experimental arrangement.

entire collimated beam. Then the collimated beam was refocused onto a liquid-helium-cooled Germanium bolometer by another f/1 parabolic mirror with a focal length of 12.8 cm.

An 8-layer metal-mesh filter was used as a low-pass filter on the input side. It has an attenuation more than 60 dB at 1 THz. A circular-waveguide array filter was used as a high-pass filter on the output side of the grid. The waveguide array filter was attached to the window of the bolometer. The circular waveguides have a diameter of  $200.7\ \mu\text{m}$  and a length of 1.02 mm. The diameter of the array is 5.1 mm. Figure 6 shows the measured transmittance of the high-pass filter from 300 GHz to 1.5 THz. The transmittance at 1 THz is 0.76 and the attenuation is more than 60 dB at 500 GHz.

## MEASUREMENT

Several different diode grids have been tested. These diode grids are glued on the edges of microscope glass slides and suspended in air. Bonding wires connect the bias lines on the substrate to the contact pads on the slides for DC biasing.

Figure 7 shows time responses of the bolometer voltage as a function of input power level. Each curve is an average of 4 pulses. The solid lines show the outputs with the multiplier grid in the path and with four different input power levels which have 0 dB, 3.8 dB, 5.8 dB and 7 dB attenuations. The dashed line was measured without the multiplier in the path and 0 dB input power attenuation. This measurement shows the harmonics are radiated from the multiplier grid instead of harmonic contamination from the free-electron laser. The 0 dB attenuation reference was

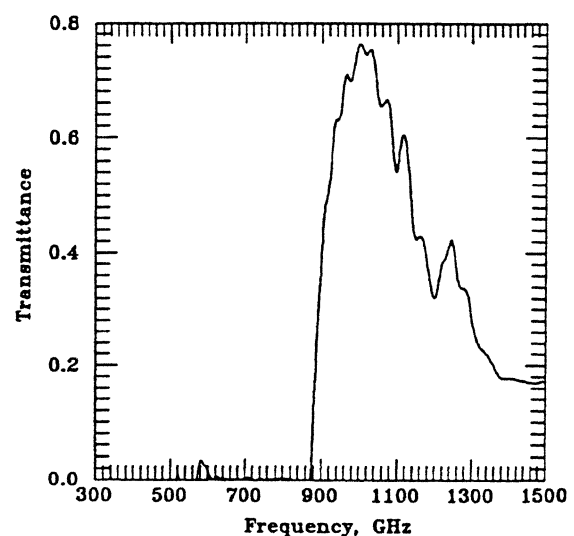


Fig. 6. Measured transmittance of the high-pass waveguide cutoff filter as a function of frequency.

actually set with enough sheets of plexiglass in front of the beam splitter so that there was no output signal detected by the bolometer without the multiplier in the optical path. Then extra attenuation was added to measure the time responses for different input signal levels.

Another way to show that the THz radiation comes

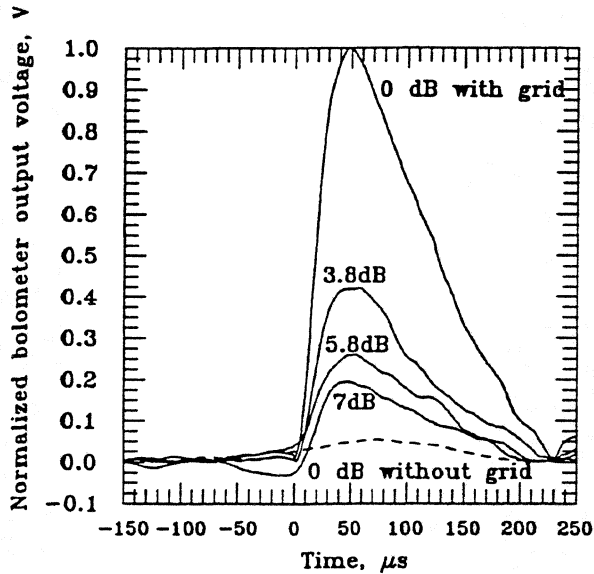


Fig. 7. Normalized time responses of bolometer voltage as a function of input power level. The dashed line was measured with 0 dB attenuation of the input power but without the multiplier in the path. The solid lines were measured with the multiplier in the path and with different attenuation of the input power.

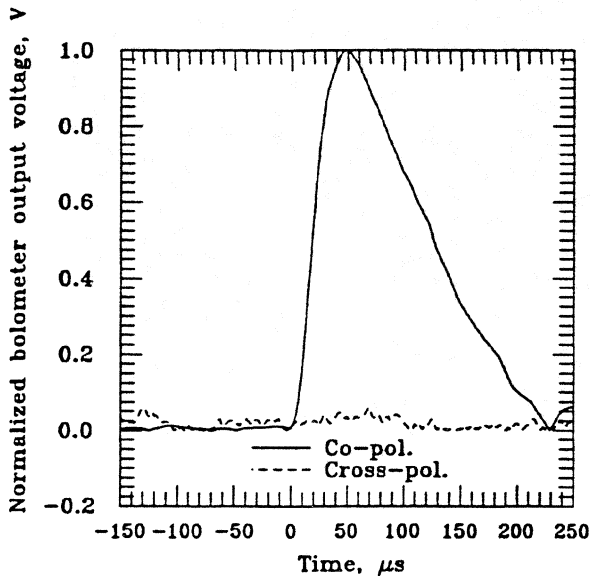
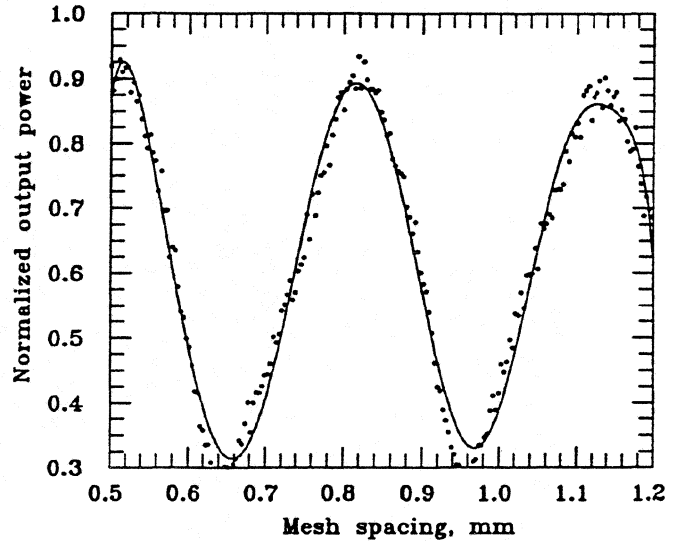
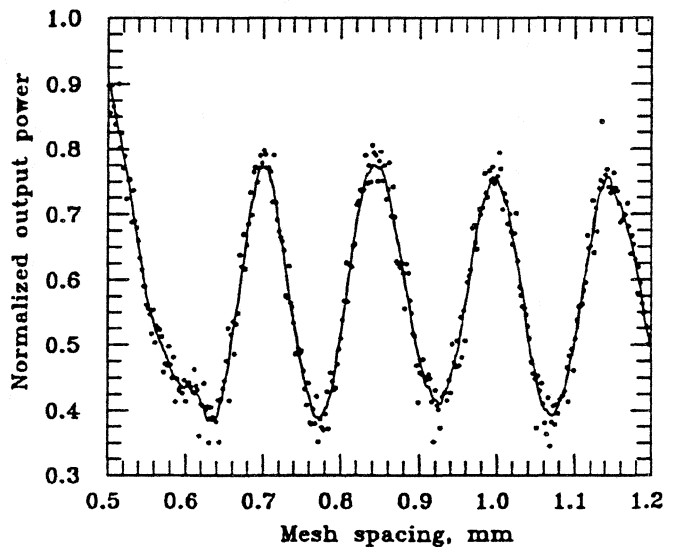


Fig. 8. Normalized time responses of bolometer voltage with different grid orientations. The solid line indicates the electric field parallel to the diode and the dashed line indicates that the electric field perpendicular to the diode.

from the grid rather than the laser is to rotate the grid by 90° and measure the cross-polarized signal. Figure 8 shows the time responses. The solid line was measured with the electric field parallel to the diodes and the dashed line was measured with the electric field perpendicular to the diodes. This result shows that: (1) The bow-tie metal structures on the grid work as linearly-polarized antennas and couple the signal into the diodes. The harmonic signal is not generated by just pumping high energy on GaAs in the device. (2) The harmonic signal does not come from the free-electron laser.



(a)



(b)

Fig. 9 Normalized output power as a function of the metal-mesh spacing in the Fabry-Perot interferometer. (a) Measurement of 500-GHz input signal and (b) measurement of 1.00 THz output signal.

A Fabry-Perot interferometer was used to measure the signal frequencies. The metal-mesh plates could be positioned in  $0.7 \mu\text{m}$  increments. Figure 9 shows (a) the fundamental frequency from the free-electron laser after passing the low-pass filter but without the high-pass filter, and (b) the output frequency from the grid after passing the high-pass filter. Figure 9(a) and 9(b) only show parts of the measured curves. The average distance between two peaks in the output-frequency measurement is  $301 \mu\text{m}$  over 14 peaks. This indicates the output frequency is  $1.00 \text{ THz}$ . No higher harmonics have been detected. The average distance between two peaks in the input-frequency measurement is  $603 \mu\text{m}$  over 9 peaks. This indicates the input frequency is  $500 \text{ GHz}$ .

## POWER

Figure 10 shows the power dependence of the first multiplier with normal incidence. This grid has diodes with an anode diameter of  $0.56 \mu\text{m}$  and 100% yield. The dashed line indicates a square-power relationship. A peak output power of  $330 \mu\text{W}$  at  $1 \text{ THz}$  was achieved when the diode grid was pumped by a peak input power of  $3.3 \text{ W}$  at  $500 \text{ GHz}$ . With low input power, the data do not follow the square-power relationship, possibly due to measurement noise. It should be noticed that these diodes have not yet saturated. We tried to increase the input power in order to investigate the saturation conditions. However, some of the diodes were damaged when the input power reached  $13 \text{ W}$ . These damaged diodes are open-circuited, verified by a curve tracer.

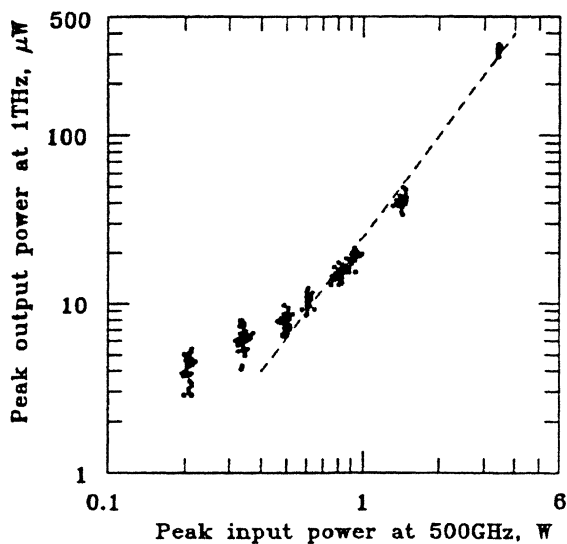


Fig. 10. Measured peak power dependence of the first multiplier grid. The dashed line indicates a square-power relationship. The diodes were not biased.

We improved the data acquisition method to investigate the power dependence with low input power. Each pulse was integrated to reduce noise effect. Because some of the diodes got damaged in the first grid, we used a new device. Figure 11 shows the power dependence of the second multiplier with normal incidence in a linear scale. This grid has diodes with an anode diameter of  $0.5 \mu\text{m}$  and 100% yield. The solid line indicates a square-power relationship. With an input power of  $800 \text{ mW}$ , this multiplier generated a peak output power of  $45 \mu\text{W}$ . These diodes have not saturated yet and some of the diodes were damaged when the input power was increased to  $4 \text{ W}$ . It should be noticed that the data with low input power follows the square-power relationship after reducing the noise effect.

## PATTERN

The diodes in the top and bottom halves of the grid have opposite polarities because the grid was designed for a sideband generator. When the grid is used as a frequency doubler, this causes an undesired null in the middle of the beam. The output pattern was measured to verify the existence of the null. The measurements were done by rotating the grid itself. In Figure 12, the solid curve shows the measured output pattern with a peak input power of  $300 \text{ mW}$ . Peaks appear at  $42^\circ$  and  $26^\circ$  from the center with a power of 3.2 times and 2.3 times bigger than the power in the null, respectively. The accuracy of this measurement is limited by the uncertainty in the position of the rotating axis. The asymmetry of the output pattern may be caused by the off-axis rotating effect or by the fact that the diodes in one array are not completely identical. The bolometer

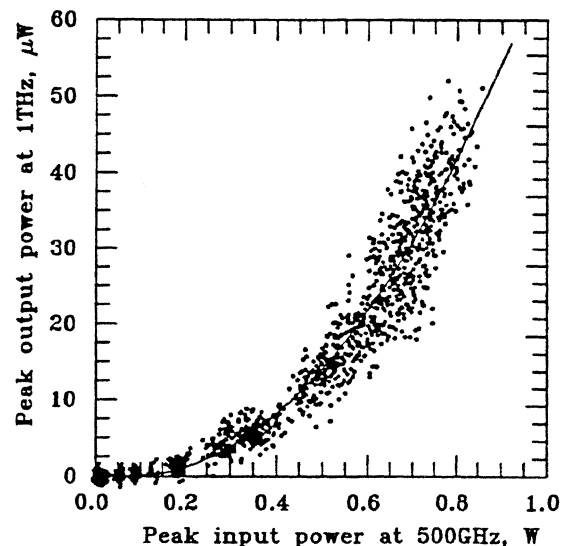


Fig. 11. Measured peak power dependence of the second multiplier grid. The solid line indicates a square-power relationship. The diodes were not biased.

has a limited acceptance angle ( $\pm 14^\circ$ ) and only 10% of the total radiated power is accepted at normal incidence. The dashed curve in Fig. 12 shows a calculated one-dimensional output pattern. Three infinitesimal current elements on the left are assumed to have an opposite phase from the other three elements on the right of a linear array and the spacing between elements is  $70 \mu\text{m}$ . The normalized array factor is determined by [13]

$$A(\theta) = \left[ \frac{\sin(\frac{3k_0 d}{2} \sin \theta)}{\sin(\frac{k_0 d}{2} \sin \theta)} \right]^2 \cdot \left[ \sin(\frac{3k_0 d}{2} \sin \theta) \right]^2 \quad (1)$$

where  $\theta$  is the angle,  $d$  is the spacing and the propagation constant  $k_0 = 2\pi / \lambda_0$  where  $\lambda_0$  is the wavelength,  $300 \mu\text{m}$ . The receiving horn in the bolometer has an acceptance angle of  $\pm 14^\circ$ . Therefore, taking both the antenna array factor and the finite acceptance-angle effect into account, the output pattern is calculated by

$$P(\phi) = \int_{\phi-14^\circ}^{\phi+14^\circ} A(\theta) d\theta \quad (2)$$

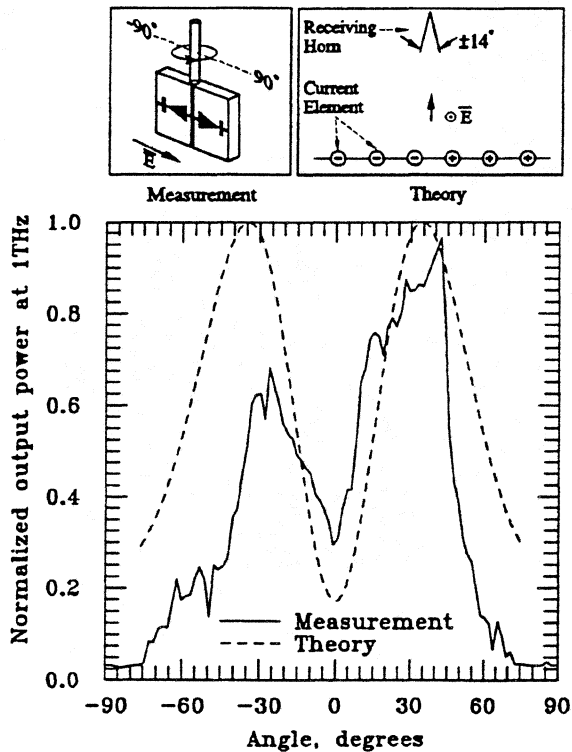


Fig. 12. Output pattern. The measurements were done by rotating the grid from  $-90^\circ$  to  $+90^\circ$  with the electric field parallel to the diodes. The solid line is a calculated output pattern considering the antenna array factor and the acceptance angle of the receiving horn. The null was caused by the opposite polarities of the diodes in two halves of the grid.

### BIASING

Traditionally, Schottky diode multipliers are reverse-biased to increase the frequency multiplying efficiency since the diodes are designed as varactors. However, these diodes were originally planned for use as sideband generators and were designed to be used under forward bias. Thus, these diodes have very thin epitaxial layers and the capacitance does not change significantly with reverse bias. Therefore, the frequency multiplication in these grids probably results from varistor multiplication, that is to say, from the nonlinear I-V relationship. C-V curves with 1 MHz RF frequency were measured by probing each diode in an array when other diodes were still connected to the one probed. The capacitance of the diodes on the edge of the array stayed the same (about 10 fF) when the bias changed from 0.4 V to  $-6$  V. The capacitance of the diodes in the center of the array varied from 19.2 fF to 18.4 fF as the bias changed from 0.4 V to  $-6$  V. These capacitances are much bigger than the estimated junction capacitance which is 0.6 fF at zero bias. The discrepancy is due to the fact that these diodes are still connected and therefore the measured capacitance is a result of all shunt capacitance in the array and the junction capacitance is not significant enough to change it when the bias changes.

Power dependence was measured under different biasing conditions. The grid was rotated to the angle where the maximum output power appeared. The maximum point of the output pattern should be more sensitive to the bias than the null in the center (with normal incidence) due to that the null is caused by a cancellation of electric fields from the two halves of the diodes. Figure 13 shows the

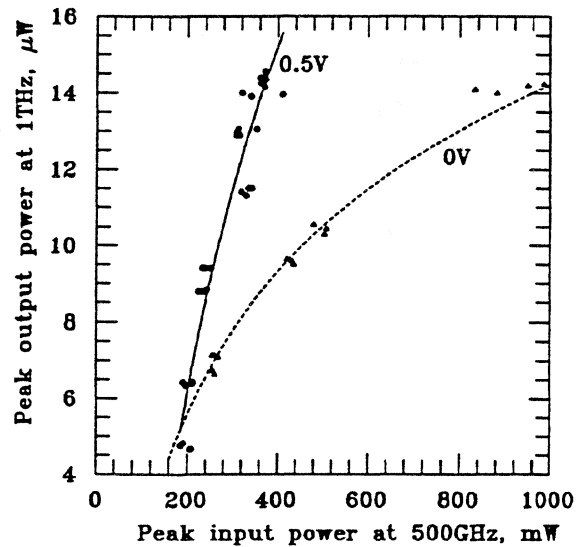


Fig. 13. Measured power dependence with bias 0 V and 0.5 V. The grid was rotated by  $30^\circ$  for the bolometer to receive signal from the peak angle of the output pattern.

measured power dependence with bias 0 V and 0.5 V. Each data point is an average of 60 pulses. The frequency doubling efficiency with a  $14 \mu\text{W}$  output power was increased from  $1.5 \times 10^{-5}$  with zero bias to  $3.9 \times 10^{-5}$  with 0.5 V bias. It should be noticed that these diodes become saturated with high input power when the diodes are biased at 0 V. This measurement verifies that the frequency multiplication results from varistors.

Peak output power was measured as a function of bias with a peak input power of 400 mW (Fig. 14). The maximum peak output power is  $17 \mu\text{W}$  with a bias of 0.375 V. Comparing with a peak output power of  $13 \mu\text{W}$  which was measured with the open-circuited bias line, it seems biasing only makes a small improvement in the output power. One possible reason is that these diodes are self-biased when the bias lines are open-circuited.

## CONCLUSION

Terahertz quasi-optical grid frequency doublers have been investigated by using Schottky diode-grids which are originally designed as sideband generators. A peak output power of  $330 \mu\text{W}$  was measured at 1 THz without any impedance tuning for  $2.42 \mu\text{s}$  500-GHz input pulses with a peak power of 3.3 W. The relationship between the input power at 500 GHz and the output power at 1 THz follows a square-power law. The polarity of the diodes designed for sideband-generator application results in a null in the center of the output beam for multiplier application. Measurements shows that only 10% of the total radiated power is received by the detector due to the null in the output beam. A grid with diode-orientation appropriate for a mul-

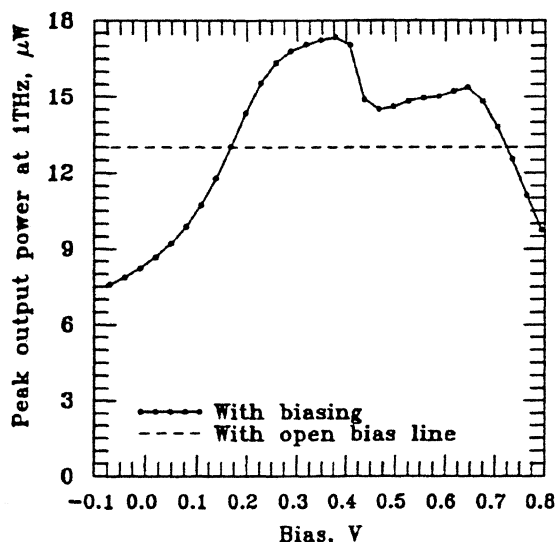


Fig. 14. Measured peak output power as a function of bias. The peak input power is 400 mW. The dashed line was measured with open-circuited bias lines.

tiplier application should improve the output pattern and increase the output power. Biasing tests verify that the frequency multiplication results from varistors. It should be possible to increase the output power and the conversion efficiency since these diodes are not saturated yet when no bias is applied.

## ACKNOWLEDGMENTS

We appreciate the support from the Jet Propulsion Laboratory and the Army Research Office. We would like to thank Jeffery Hesler and Dr. William Bishop for their help on fabrication at University of Virginia. We would also like to thank David Enyeart and the staff of the Center for Free-Electron Laser Studies for their help on operating the laser at University of California, Santa Barbara. We are grateful to Kent Potter for his help building the measurement components and Michael DeLisio for valuable discussion at California Institute of Technology.

## REFERENCES

- [1] T.G. Phillips, "Developments in Submillimeterwave Astronomy," *The 19th International Conference on Infrared and Millimeter Waves*, Sendai, Japan, Oct. 1994.
- [2] J.W. Waters and P.H. Siegel, "Applications of Millimeter and Submillimeter Technology to Earth's Upper Atmosphere: Results To Date and Potential for the Future," *The 4th International Symposium on Space Terahertz Technology*, Los Angeles, CA, March 1993.
- [3] M.A. Frerking, "The Submillimeter Mission Heterodyne Instrument," *The Proceeding of the 2nd International Symposium on Space Terahertz Technology*, pp. 17-31, 1991.
- [4] A. Rydberg, B.N. Lyons and S.U. Lidholm, "On the Development of a High Efficiency 750 GHz Frequency Tripler for THz Heterodyne Systems," *IEEE Trans. on Microwave Theory and Tech.*, vol. 40, No. 5, pp. 827-830, May 1992.
- [5] N. Erickson and J. Tuovinen, "A Waveguide Tripler for 800-900 GHz," *The 6th International Symposium on Space Terahertz Technology*, Pasadena, CA, March 1995.
- [6] R. Zimmermann, T. Rose and T. Crowe, "An All Solid-State 1 THz Radiometer for Space Applications," *The 6th International Symposium on Space Terahertz Technology*, Pasadena, CA, March 1995.
- [7] Jonathan B. Hacker, "Grid Mixers and Power Grid Oscillators," *Ph.D. Dissertation*, California Institute of Technology, 1994.
- [8] J.B. Hacker, R.M. Weikle II, M. Kim, M.P. DeLisio, D.B. Rutledge, "A 100-Element Planar Schottky Diode Grid Mixer," *IEEE Trans. Microwave Theory Tech.*, vol. 40, no. 3, pp. 557-562, March 1992.

- [9] C.F. Jou, W.W. Lam, H.Z. Chen, K.S. Stolt, N.C. Luhmann, Jr. and D.B. Rutledge, "Millimeter-Wave Diode-Grid Frequency Doubler," *IEEE Trans. on Microwave Theory and Tech.*, vol. 36, No. 11, pp. 1507-1514, Nov. 1988.
  - [10] H-X.L. Liu, L.B. Sjogren, C.W. Domier, N.C. Luhmann, Jr., D.L. Sivco and A.Y. Cho, "Monolithic Quasi-Optical Frequency Tripler Array with 5-W Output Power at 99 GHz," *IEEE Electron Device Letters*, vol. 14, No. 7, pp. 329-331, July 1993.
  - [11] T.W. Crowe, R.J. Mattauch, H.P. Röser, W.L. Bishop, W.C.B. Peatman and X. Liu, "GaAs Schottky Diodes for THz Mixing Applications," *Proceedings of the IEEE*, vol. 80, No. 11, pp. 1827-1841, Nov. 1992.
  - [12] S.J. Allen, K. Craig, B. Galdrikian, J.N. Heyman, J.P. Kaminski, K. Campman, P.F. Hopkins, A.C. Gossard, D.H. Chow, M. Lui and T.K. Liu, "Materials Science in the Far-IR with Electrostatic Based FELs," presented at *FEL 94*, Stanford, CA, August 1994.
  - [13] D. Cheng, "Field and Wave Electromagnetics," *Addison-Wesley Pub. Co.*, Chap. 11, 1983.
-